Influence of zirconium propoxide on the radical induced photopolymerisation of hybrid sol–gel materials

Davy-Louis Versace, Olivier Soppera, Jacques Lalevée and Céline Croutxé-Barghorn*

Received (in Montpellier, France) 10th April 2008, Accepted 3rd June 2008
First published as an Advance Article on the web 18th September 2008
DOI: 10.1039/b806056h

This study emphasizes the role of zirconium propoxide on the free-radical photopolymerisation of hybrid organic–inorganic material based on 3-methacryloxypropyltrimethoxysilane (MAPTMS). By means of atomic force microscopy in pulsed force mode and real-time Fourier-transform infrared spectroscopy, it is shown that the addition of zirconium complex in the hybrid sol–gel material leads to a well-polymerised and hydrophilic surface under UV-illumination. By contrast, sols without zirconium complex exhibit soft and sticky surfaces. The study also demonstrates an unexpected role of oxygen in the photopolymerisation process. Indeed oxygen is well-known being a strong inhibitor of the radical polymerisation. However, in the present case, it interacts with $Zr(OPr)_4$ and participates in a positive way to the photochemical process. During the irradiation, radicals react with O_2 to form peroxyl radicals that are generally inert towards the photopolymerisation. By using laser flash photolysis, it was proved that these radicals combine with zirconium propoxide to form new initiating species that contribute to further free-radical photopolymerisation.

Introduction

Mixing two different components with a view to combine their properties (namely thermal, mechanical or optical properties) is an attractive idea but not easy to apply. Indeed, the combination of two materials with different properties generally gives rise to incompatibilities in terms of solubility. In this sense building a homogeneous hybrid material is a challenge for the scientist community.

In this context, sol–gel processing has aroused interest the last 10 years and represents a creative alternative to design new compounds for industrial and academic researches and innovations, as attested by the rapid growth of studies in this field.[1–4] The hybrid organic–inorganic materials clearly appear appropriate candidates to the current trend.

One of the most promising applications takes place in the field of protective and functional coatings for organic and inorganic substrates.[5,6] In particular, the sol–gel process allows the formation of inorganic layers at temperatures much lower than those of the degradation of the organic components. The application of these coatings to polymer substrates is particularly attractive to give them attractive properties such as scratch resistance,[7] abrasion resistance,[8,9] barrier properties.[10] Among the most remarkable features, it is interesting to mention corrosion protection[11–13] for aluminum alloy surfaces, high barrier properties towards liquid and volatile compounds,[14] water vapor oxygen or flavor permeation,[15,16] photonic applications[17–19] or antibacterial activity[20] *etc*.

Département de Photochimie Générale, CNRS UMR no. 7525, 3 rue Alfred Werner 68093 Mulhouse Cedex France. E-mail: Celine.Croutxe-Barghorn@uha.fr; Fax: +33 389 335 014; Tel: +33 389 335 017

Hybrid components are separated into two classes:[21] in class I, organic and inorganic compounds are mixed together and only weak bonds (hydrogen bonding, van der Waals or ionic bonds) give cohesion to the whole structure. In class II, the two phases are linked together through strong chemical bonds (covalent or iono-covalent bonds).

Among the available commercial class II precursors, 3-methacryloxypropyltrimethoxysilane (MAPTMS) has been thoroughly investigated.[22–27] Starting from this precursor, material elaboration is achieved by the classical sol–gel route that forms an inorganic network at room temperature by the hydrolysis and condensation of alkoxy compounds, The organic moiety, a methacrylate function, can react *via* a free-radical polymerisation mechanism initiated by UV-light to lead to a polymethacrylate network within the silicate backbone. The final properties of this kind of materials combine both the polymer qualities (suppleness) and the characteristics of a glass (mechanical and thermal resistance). In addition, photochemical treatment offers many advantages over the thermal curing, such as fast curing, low-energy consumption, spatiotemporal control of the reaction, elimination of a costly thermal drying and finally the cycle time for each coated part could be cut dramatically.[28] Further, mechanical or optical properties can be tuned by the incorporation of other metal alkoxides[22,29] (Ti, Zr, Al, *etc*.).

Up to now, few studies concerning the photopolymerisation process and its impact on the local mechanical properties of the hybrid sol–gel materials have been done:[30] It has been shown that strong interactions exist between the inorganic network structure and the polymerisation of the organic component. Furthermore, the condensation of the silicate backbone can enhance the conversion of organic reactive functions. The most surprising result is the role played by

the titanium alkoxide in the photopolymerisation process and on the surface properties of the corresponding photopolymerised films: titanium components participate to the photochemical process, lead to the formation of active radical species that counterbalance the well known inhibition effect of O_2 in radical polymerisation. They are involved in a surface becoming more hydrophilic, as demonstrated by atomic force microscopy (AFM) in pulsed force mode.[31]

As regards to the role of zirconium alkoxides on the photopolymerisation process in hybrid sol–gel materials, no further study has been conducted. Some papers proved that zirconium alkoxides could be used such as thermal polymerisation initiators[32,33] but the catalytic effect of zirconium, under air conditions, in UV photopolymerisation, and the coupling reaction with radicals were not investigated.

In this context, the present study focuses on the effect of zirconium propoxide on the photochemical reactions and the film surface modifications under UV light. A relation between the photopolymerisation of the cured films and the local mechanical properties under different atmospheres and for various zirconium alkoxides ratios was established. Real-time Fourier-transform infrared spectroscopy, coupled with AFM in pulsed force mode[30,34] allowed to correlate the conversion of reactive functions to local mechanical characterisation of the cured samples. Finally, a mechanistic approach concerning the reaction between zirconium propoxide and oxygen was carried on by laser flash photolysis.[35]

Experimental

Sol–gel materials

Sol preparation. The synthesis of the sol–gel matrix was based on the formation of a stable and homogeneous sol obtained from the mixture of a photosensitive organically modified silane, 3-methacryloxypropyltrimethoxysilane (MAPTMS, Assay ~99%, Aldrich), zirconium(IV) *n*-propoxide ($Zr(OPr)_4$, Assay ~70% in propanol, Aldrich) and methacrylic acid (MAAH, $C_4H_6O_2$, Assay >98%, Aldrich). The difference in reactivity between these alkoxides implies a three-step process as sketched in Fig. 1. MAPTMS (3 g, 12 mmol) was first pre-hydrolysed with an aqueous solution (0.16 mL, 0.1 M HCl), employing a 1 : 0.75 water to alkoxide ratio. As MAPTMS and water are not miscible, the hydrolysis was performed in a heterogeneous manner. After 20 min stirring, the production of methanol became sufficient to allow the miscibility of all species introduced in solution. To control the hydrolysis–condensation of $Zr(OPr)_4$, MAAH was used to covalently chelate the zirconium. This was done by employing a stoichiometric molar ratio of chelating agent to the zirconium alkoxide.

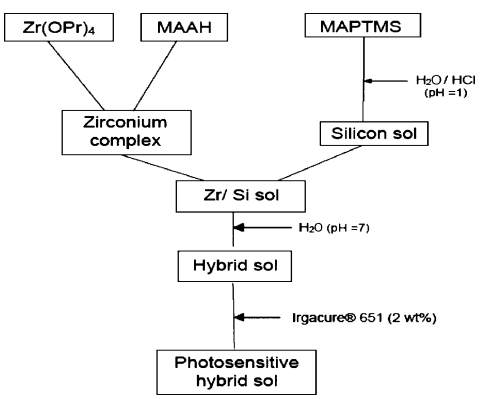

Fig. 1 Sol–gel synthesis of the photosensitive hybrid sols.

Table 1 Composition of the photosensitive hybrid formulations

	Molar ratio			
Material	Sol 1	Sol 2	Sol 3	Sol 4
MAPTMS	10	10	10	10
$Zr(OPr)_4$	—	1	2	4
MAAH	—	1	2	4
H_2O	20	20	20	20
Irgacure® 651	0.2	0.2	0.2	0.2

After 45 min of reaction, the pre-hydrolysed MAPTMS solution was added dropwise to the zirconium complex in order to avoid any precipitation. The last step consisted in introducing water (0.3 mL, pH = 7) in the resulting mixture to perform the hydrolysis of the sols. The final water : alkoxide molar ratio is 2 : 1 in the sols. The sol was left stirring for 24 h before addition of the photoinitiator, Irgacure® 651, a 2,2-dimethoxy-2-phenyl acetophenone[36] provided by Ciba Specialty Chemicals Co. All of the sols contain 2 wt% of Irgacure® 651 (60 mg, 0.23 mmol) with regard to MAPTMS and all chemicals were used without any further purification.

For the purpose of this study, four mixtures containing different concentrations of zirconium complex were investigated. The molar ratio MAPTMS/Zr as well as the characteristics of these formulations are listed in Table 1. In addition, a sol without any zirconium complex was prepared as reference.

Hybrid film photopolymerisation

The sol–gel material was coated onto silicon substrates (previously cleaned with ethanol and acetone) and spin-coated using a Suss Microtec Delta10TT spin-coater. A spinning rate of 1000 rpm during 30 s allowed to prepare films with a thickness of 11–12 μm, which is suitable for RT-FTIR and pulsed force mode characterisations. The liquid films were then polymerised under UV irradiation in order to obtain a dry coating.

Characterisation methods and procedures

UV-visible. The UV-visible absorption spectra (200–800 nm) of the photosensitive sols were obtained using a Beckman DU-640 Spectrophotometer. Formulations were filled into a 500 μm path cell.

Real-time Fourier-transform infrared spectroscopy. The kinetics of the radical photopolymerisation of the sols were followed by real-time Fourier-transform infrared spectroscopy. This technique is sensitive, non-destructive and usually used to monitor structural and compositional changes.[37,38]

The infrared absorption spectra were recorded by a FTIR spectrometer (model Vertex 70, Bruker) with a resolution of 4 cm^{-1}. All the infrared experiments described in this study were performed at room temperature with UV light emitted by an Hg–Xe arc source (Hamamatsu L8222-01) equipped with a waveguide. The intensity of the UV light was adjusted to 83 mW cm^{-2}. The infrared analysis was carried out both under atmospheric and laminated conditions (a polypropylene film was put on the top of the photosensitive layer).

The progress of the polymerisation of the organic component was determined by monitoring the decrease of the 1636 cm^{-1} band corresponding to the C=C bond of the methacrylate function of the MAPTMS precursor. After baseline correction, the conversion ratio χ_c of the functional group can be calculated after measurement of the absorbance at each time of the reaction as follows (eqn (1)):

$$\chi_c(\%) = \frac{A_0^{1636} - A_t^{1636}}{A_0^{1636}} \times 100 \qquad (1)$$

where χ_c is the conversion ratio of these reactive functions at time t, A_0 is the initial absorbance (before UV irradiation) and A_t is the absorbance of the functional groups at time t.

The rate of polymerisation (R_p) can be easily determined at any stage of the reaction from the slope of the kinetic curve $d\chi_c/dt$ and the initial concentration of the photoreactive group ($[M_0]$ in mol l^{-1}) (eqn (2)):

$$R_p = \frac{[M_0]}{100}\left(\frac{d\chi_c}{dt}\right) \qquad (2)$$

^{29}Si nuclear magnetic resonance spectroscopy. ^{29}Si NMR study was performed on a Bruker MSL 400 spectrometer. Liquid ^{29}Si NMR experiments (79.48 MHz) were recorded at room temperature (293 K). $T1$ measurements made on the unhydrolysed monomers show that 15 s recycle delay time and a 6.6 μs-pulse duration (π/4 excitation pulse) were sufficient for quantitative measurements. Sols, introduced in a 8-mm tube, were inserted into a 10-mm tube containing $CDCl_3$ as an internal lock and tetramethylsilane (TMS) as a reference. The chemical shifts were given in parts per million (ppm) relative to TMS. Sixty-four scans were accumulated for each spectrum. ^{29}Si NMR spectra modeling was done with the Winfit program[39] to estimate the species distribution. Chemical shift of Si is directly linked to the close environment of the Si atom. In the case of trifunctional alkoxysilanes R–Si(OR′)$_3$, the chemical shifts of silicium range between −30 and −70 ppm. In this range, four groups corresponding to the different environments of the silicium are observed. The conventional T^n notation, where T represents a silicon atom and n the number of bridging oxygen atoms is used to describe the inorganic network of hydrolyzed and condensed monomers. According to this notation, T^0 represent monomeric groups, T^1 end groups of chains, T^2 middle groups in chains or cycles and T^3 fully branched sites.

Atomic force microscopy/pulsed force mode. Photopolymerised films were investigated by atomic force microscopy (AFM). The atomic force microscope was a PicoPlus from Molecular Imaging. The pulsed force mode was provided by an external unit from WITEC Company. The tips were Silicon-FM Pointprobes from Scientec-Nanosensors with a resonant frequency at *ca.* 70 kHz (force constant: 2 N m^{-1}). The pulsed force mode controller introduces a sinusoidal modulation of the z-piezoelectric transducer (Z-PZT) with an amplitude of typically 10–500 nm at a user-selectable frequency between 100 Hz and 2 kHz (which is far below the resonance frequency of the cantilever) to bring the tip in and out of contact with the sample. The amplitude of oscillation was adjusted so that the tip was out of contact with the sample at the lowest point of the oscillation and reached a defined maximum deflection at the highest point of the oscillation. In this study, the pulsed force mode signal throughout a cycle was recorded *via* a PC acquisition card. It is a non-resonant mode designed to allow approach curves to be acquired along the scanning path. It thereby provides the topography of the sample and extends the possibilities of the prevalent contact and intermittent-contact AFM modes to a direct and simple local characterisation of adhesion and stiffness. The theoretical background concerning pulsed force mode measurements is well described in previous papers.[30,31,34] The signal was recorded in different locations of the samples in order to get an average response within the whole surface. From the slope of the signal, information on the stiffness and adhesion of the film can be collected. Sols with different Si : Zr ratios were characterised and compared.

Laser flash photolysis set-up. It has been recently shown that laser flash photolysis was suitable for the direct observation of peroxyl radicals[40] (ROO$^\bullet$) resulting from the interaction of radicals (R$^\bullet$) generated upon UV irradiation to oxygen. The experimental procedure requires the formation of *tert*-butoxyl radical (**B**) from the irradiation of di-*tert*-butyl peroxide (**A**) at 355 nm (Fig. 2). This radical reacts with triethylamine (TEA, **C**) to generate an aminoalkyl radical (TEA$^\bullet$, **D**). The aminoalkyl radical leads in presence of O_2 to the peroxyl radical TEA-$O_2^\bullet$ (**E**), which exhibits a very long lifetime (4 ms) and absorbs at 380 nm. Therefore, laser flash photolysis was used to investigate the interactions between peroxyl radicals formed during the irradiation of the hybrid sol gel material and the zirconium complex. The absorbance decay of the peroxyl radicals was followed at 380 nm.

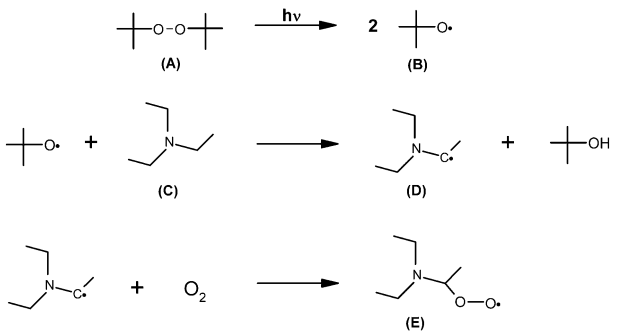

Fig. 2 Procedure for the production of peroxyl radicals in an oxygen-saturated solution: (**A**) di-*tert*-butyl peroxide, (**B**) *tert*-butoxyl radical, (**C**) triethylamine, (**D**) aminoalkyl radicals, (**E**) adduct product.

The nanosecond transient absorption setup working at 355 nm is based on the nanosecond Nd:YAG laser (Powerlite 9010, Continuum) operating at 10 Hz with an energy decreased down to 7 mJ pulse^{-1} at 355 nm as the excitation laser. This system (LP900, Edinburgh Instruments) used a 450-W pulsed xenon arc lamp, a Czerny–Turner monochromator, a fast photomultiplier, and a transient digitizer (TDS 340, Tektronix). The beam irradiated a 1-cm cell containing the formulation. Measurements were done at room temperature.

Computational procedure. Molecular orbital calculations were carried out with the Gaussian 03 suite of programs.[41] The reaction enthalpies (ΔH_r) of the investigated reactions were determined at UB3LYP/LANL2DZ level (with ZPE correction).

Results and discussion

Influence of the MAPTMS : zirconium complex molar ratio

Structure of the inorganic network. The structural evolution of the inorganic part of the different formulations, at room temperature, was first investigated by Fourier-transform infrared spectroscopy and silicium nuclear magnetic resonance spectroscopy (^{29}Si NMR) in the liquid state, which is also an appropriate technique to describe the condensation state of the silicate network. The chemical control of metal transition alkoxide hydrolysis and condensation reactions was achieved by complexation with a carboxylic acid (MAAH) that promotes the preparation of stable, uniform and transparent sols. Under the stoichiometric molar ratio between $Zr(OPr)_4$ and MAAH used in this study, there are still some free zirconium propoxide molecules in the sols. Fig. 3 exhibits an overview of the infrared spectra of the sols spin-coated onto the silicon wafer before the UV irradiation. The vibration band corresponding to Zr–OPr bond can be identified in sols 2–4 at 1006 cm^{-1} showing that hydrolysis of free $Zr(OPr)_4$ is limited. A broad band at 3425 cm^{-1} and a band at 910 cm^{-1} can be identified and are attributed to the presence of free silanols[42,43] (ν(Si–OH)). These band absorbances are twice as high in sol 1 (without $Zr(OPr)_4$) compared to the other sols.

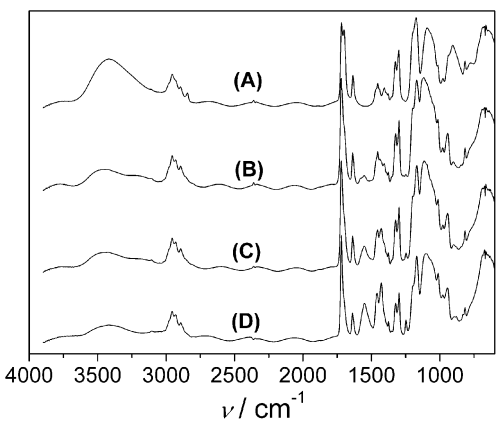

Fig. 3 Overview of the infrared spectra of the different formulations spin-coated onto silicon wafer with (A) sol 1, (B) sol 2, (C) sol 3 and (D) sol 4. Sols are aged for 1 day at room temperature.

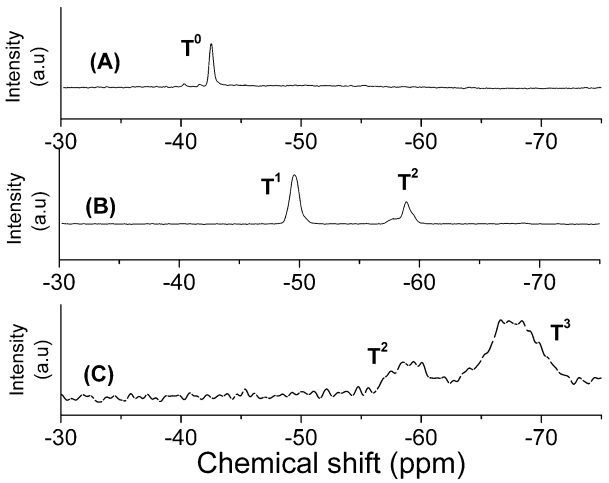

Fig. 4 Liquid ^{29}Si NMR spectra of (A) monomer MAPTMS, (B) sol 1 and (C) sol 4 after 24 h ageing at room temperature.

The broad band between 1000 and 1150 cm^{-1} corresponds to the –Si–O–Si– asymmetric stretching.[44] For sols 2, 3 and 4, this band appears larger and the corresponding peak absorbance is higher than in sol 1.

These results clearly demonstrate that inorganic network is more condensed in $Zr(OPr)_4$/MAAH containing sols. ^{29}Si NMR results (Fig. 4) confirm the trend observed with FTIR: for sol 1, the percentage of T^1 and T^2 species are, respectively, 58 and 42% whereas in sol 4, T^1 species totally disappear and only T^2 (24%) and T^3 (76%) species remain.

The addition of $Zr(OPr)_4$ /MAAH complex contributes to a rapid consumption of the silanol group (Si–OH), resulting from the hydrolysis of MAPTMS, and the creation of siloxane bonds, as a consequence of the condensation of MAPTMS.

Fig. 5 displays the influence of the MAPTMS : zirconium molar ratio on the frequency characteristics of the $Zr(OPr)_4$/MAAH complex. Vibration bands were identified at 1580, 1550 and 1460, 1427 cm^{-1} for the antisymmetric and symmetric stretching frequencies[45] of the MAAH acetate group, respectively. According to the MAPTMS : zirconium molar ratio, different coordination modes can be adopted by the carboxylate ligands (monodentate, bidentate bridging and

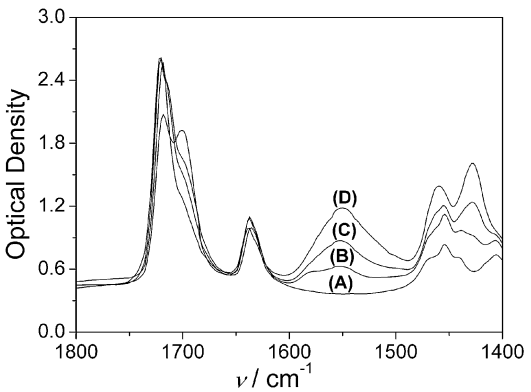

Fig. 5 Influence of the MAPTMS : zirconium complex molar ratios on the frequency vibration mode characteristics of the zirconium propoxide/MAAH complex at room temperature: (A) sol 1, (B) sol 2, (C) sol 3 and (D) sol 4. Sols are aged for 1 day at room temperature.

bidentate chelating). As reported in some studies,[46,47] methacrylic acid is bonded to zirconium atom as a bidentate chelating ligand and the frequency difference between $\nu(COO)_{asym}$ and $\nu(COO)_{sym}$ is 100 cm^{-1}. For sol 2, two bands appear at 1580 and 1550 cm^{-1} but only the one at 1580 cm^{-1} disappears by increasing zirconium propoxide concentration. According to these results, MAAH can adopt three coordination modes in sol 2, namely monodentate, bidentate bridging and bidentate chelating. For both sols 3 and 4, it is likely that all methacrylate groups are in a chelating or bridging coordination mode.

It can be also noticed that the hydrogen-bonded interactions between the acrylate carbonyl group and the acidic silanol group,[43] expressed by a shoulder at 1700 cm^{-1}, decreases from sol 1 to sol 4 as the consequence of the increased condensation of the inorganic network.

Kinetics of photopolymerisation and characterisation of the cured films by pulsed force mode. Low molecular weight organoalkoxysilanes $R'Si(OR)_3$ used as precursor for the sol–gel reaction allow to produce a liquid organic-based polysiloxane network at the end of the maturation time (24 h). After this preliminary step, sols coated onto substrates were exposed to UV irradiation in order to obtain a final dry-coating. This subsequent photopolymerisation affords a solid cross-linked organic–inorganic system.

Kinetics of photopolymerisation for the different photosensitive formulations are reported in Fig. 6. Table 2 displays both the final conversion ratio and the surface characteristics of these films for different irradiation times.

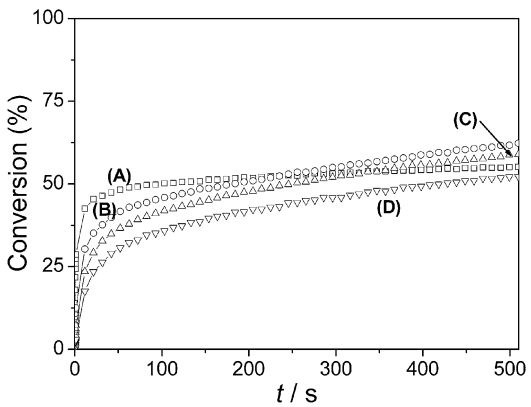

Fig. 6 Photopolymerisation kinetics of the different formulations under atmospheric conditions at room temperature: (A) sol 1, (B) sol 2, (C) sol 3 and (D) sol 4.

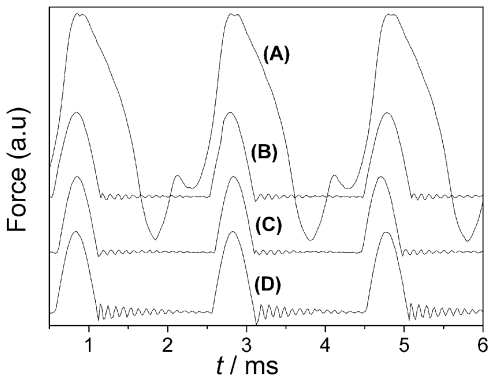

Fig. 7 Pulsed force mode signals of the cured films after 510 s irradiation at room temperature: (A) sol 1, (B) sol 2, (C) sol 3 and (D) sol 4.

These results demonstrate that the final conversion ratio is almost independent of the presence of zirconium propoxide. In all cases, after 510 s irradiation, a conversion ranging from 50 to 60% was reached, which is in good agreement with the data already reported in the literature.[23,24] The decrease in polymerisation rate from sol 1 to sol 4 is attributed to the decrease in photoinitiator concentration in the formulations. Indeed, an UV absorption difference appears between sol 1 and sol 4 in the Irgacure® 651 absorption region: the optical density of sol 1 is almost twice as high than in sol 4. This difference can be explained by a dilution effect of a factor 1.8 of the photoinitiator.

Photopolymerised films were investigated by atomic force microscopy in pulsed force mode for different illumination times (15, 200 and 510 s).

Interestingly, the pulsed force mode response of the films after 510 s irradiation (end of the kinetic study) was found to strongly depend on the content of the $Zr(OPr)_4$/MAAH complex (Fig. 7).

For sol 1, a signal very different from the typical pulsed force mode response was recorded. Such a signal corresponds to a very soft and sticky surface and characterizes a surface with very low polymerisation. The greater amplitude of the signal is thus not significant. This result is in accordance with the observation of a tacky surface. The addition of $Zr(OPr)_4$, even at low content, allows switching to a non-sticky surface, as demonstrated by the pulsed force mode signal. It is worth noting that the polymerisation process is not characteristic of the global conversion ratio of the whole layer determined by infrared spectroscopy. Even if the final conversion ratios of the investigated sols range between 52 to 62% (for 510 s

Table 2 Final conversion ratio (%) of the different formulations after 15, 200 and 510 s irradiation under atmospheric conditions, at room temperature, and surface characterisation of the cured samples as determined by atomic force microscopy in pulsed force mode

	Sol 1		Sol 2		Sol 3		Sol 4	
Irradiation time (s)	Final conversion ratio (%)	Surface characterization	Final conversion ratio (%)	Surface characterization	Final conversion ratio (%)	Surface characterization	Final conversion ratio (%)	Surface characterization
15	48	Tacky	32	Tacky	25	Tack free	18	Tack free
200	57	Tacky	49	Tack free	48	Tack free	42	Tack free
510	55	Tacky	62	Tack free	59	Tack free	52	Tack free

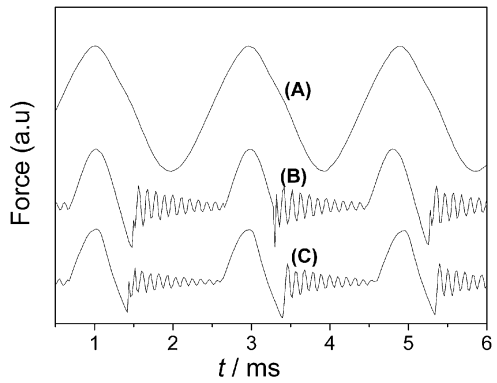

Fig. 8 Pulsed force mode signals of the cured films after 15 s irradiation at room temperature: (A) sol 2, (B) sol 3 and (C) sol 4.

illumination time), the polymerisation process at the surface of the film can be highly inhomogeneous due to the presence of oxygen that inhibits the radical polymerisation and leads to a gradient of conversion within the film.

The same trend in pulsed force mode response was observed for 200 s irradiation time. The approach of the atomic force microscopy tip to the surface was not even possible for sol 1 because the surface remained liquid provoking a crash of the tip due to the capillarity force. The adhesion peak becomes stronger when the content of $Zr(OPr)_4$ increases. This result can be attributed to the presence of $Zr(OPr)_4$ that leads to an increase in condensation of the inorganic backbone in which Si–O–Zr bonds can be formed.[48,49] Since these bonds are known to be relatively unstable,[48] Si–OH and Zr–OH bonds can be generated during irradiation, under atmospheric conditions, giving rise to a more hydrophilic surface responsible for greater adhesion.

For the pulsed force mode signals after 15 s irradiation (Fig. 8), sols 3 and 4 exhibit a tack free surface although the conversion ratio does not exceed 25%. It appears that there is a limitation of the oxygen inhibition at the film surface for $Zr(OPr)_4$ formulations. Interestingly, the adhesion is higher for 15 s than for 200 or 510 s. In this case, the indentation depth is greater for low irradiation time due to the lower reticulation of the organic network. In consequence, the pull off force is more important since the contact surface between the tip and the surface increases.

Influence of the atmosphere on the pulsed force mode signals and photopolymerisation

Due to the fast diffusion of oxygen from the atmosphere, inhibition of the polymerisation is the most pronounced at the surface of the photosensitive film. Therefore, it was interesting to compare the pulsed force mode response of the films photopolymerised under air atmosphere and laminated conditions as a function of the MAPTMS : zirconium complex ratio. Laminated conditions avoid diffusion of atmospheric oxygen within the sample and were achieved by putting a polypropylene film (also transparent to the UV radiation in the considered IR range) on the top layer of the liquid film. Fig. 9 displays the photopolymerisation kinetics of both sols (1 and 4) under air and laminated conditions and Fig. 10 presents the pulsed force mode response. Table 3 summarises

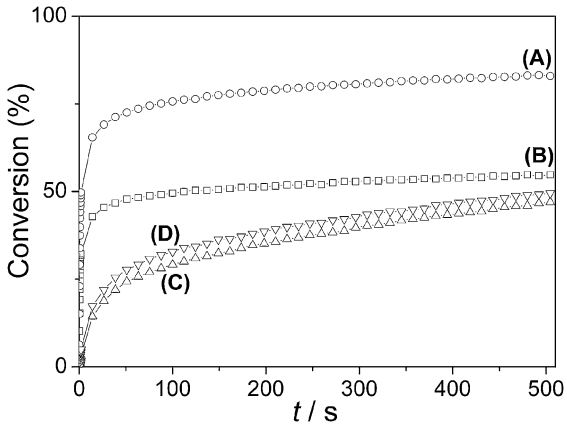

Fig. 9 Photopolymerisation kinetics of (A) sol 1 in laminated condition, (B) sol 1 under air condition, (C) sol 4 under air condition and (D) sol 4 under laminated condition at room temperature.

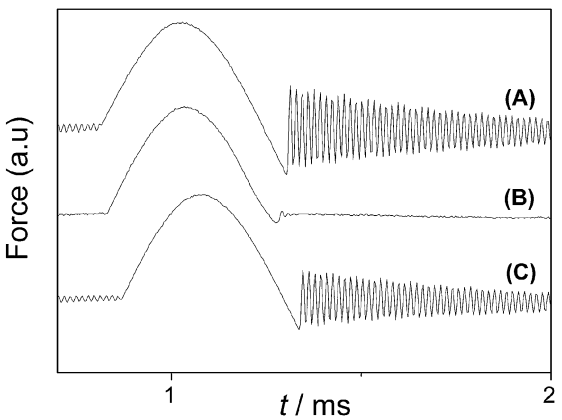

Fig. 10 Pulsed force mode response of the cured films, after 510 s irradiation, corresponding to: (A) sol 1 in laminated condition, (B) sol 4 in laminated condition and (C) sol 4 under air condition.

the corresponding final conversion ratios and the polymerisation rates.

For sol 1, the results are in accordance with those obtained for all organic formulations.[23,24] Indeed, in a laminated sol, the final conversion rate reaches 83% and drops to 55% under atmosphere conditions. The free radicals created from the photolysis of Irgacure® 651 at room temperature, under air conditions, are not efficient enough to counterbalance the oxygen inhibition and the initiating process is reduced. The polymerisation rate in sol 1 is effectively more important in a laminated sol. More surprisingly are the results for sol 4. There is no significant increase in $R_p/[M_o]$ for the laminated film in comparison with the air-cured film. In addition, the

Table 3 Rate of polymerisation ($R_p/[M_o]$ in s^{-1}) and final conversion ratio (%) of sols 1 and 4 after 510 s irradiation under laminated and atmospheric conditions

	Sol 1		Sol 4	
	Air	Laminated	Air	Laminated
$R_p/[M_o]$ ($\times 100\ s^{-1}$)	30.5	42	1.6	2.4
Final conversion ratio (%)	55	83	47	50

polymerisation rates in sol 4 (laminated or air condition) are 15 to 20 times lower those in sol 1. Further, the final conversion ratios in both laminated and air formulations are similar (around 50% after 510 s irradiation).

The results of pulsed force mode experiments (Fig. 10) seem to demonstrate a significantly different reactivity towards oxygen linked to the presence of zirconium complex. Polymerisation of sol 1 under laminated conditions leads to pulsed force mode signals that correspond to a well-crosslinked surface. It is interesting to note the presence of adhesion of the film, which can be interpreted by the hydrophilic properties of the hybrid film due to the Si–OH bonds.

The photopolymerisation of laminated sol 4 film as expected produced a well-crosslinked surface. However, its adhesion is low. On the contrary, under atmospheric conditions, the adhesion peak increases. These results tend to demonstrate that the origin of the hydrophilic properties of the film is linked to an interaction between the zirconium complex and the atmosphere.

Mechanistic approach of zirconium effect for polymerisation under air

The tacky surface is attributed to the reaction of O_2 with the initiating and propagating radicals that form peroxyl radicals. These latter are unreactive toward double bonds and so the polymerization is inhibited. As regards to the photopolymerisation and pulsed force mode results, the addition of zirconium complex leads to tack-free surface after photopolymerisation under atmospheric conditions. It seems that a mechanism involving these species contributes to reduce O_2 inhibition at the sample surface. With a stoichiometric ratio between $Zr(OPr)_4$ and MAAH, some zirconium propoxide molecules are expected to be free in formulations and the following mechanistic approach only considers such zirconium propoxide molecules. At first glance, this effect may be attributed to the reaction of zirconium complex with peroxyl radicals. In order to confirm this hypothesis, the reactivity of an observable peroxyl radical formed from an aminoalkyl radical (TEA-$O_2^{\bullet}$) was studied by laser flash photolysis. This is a technique which involves the observation, through absorption or emission, of an excited state generated by an intense pulse of laser radiation.[35] At a given wavelength, using a fixed time window, the evolution of the absorbance of the short-lived intermediates can be examined. Photochemical phenomena such as quenching reactions of transients lead to the comprehension of photophysical mechanisms.

Fig. 11 exhibits the reaction of the peroxyl radicals TEA-$O_2^{\bullet}$ by addition to the zirconium complex. Experiments were conducted in the presence of a small amount of propanol, which is the solvent of $Zr(OPr)_4$. This compound does not interfere with the mechanism depicted in Fig. 12. Indeed, the reaction rate between peroxyl radicals and a proton resulting from H abstraction on propanol is very slow. Therefore, it cannot compete with the proposed mechanism.[50]

Addition of $Zr(OPr)_4$/MAAH complex drastically affects the observed peroxyl kinetics: both the quantum yield and the lifetime of TEA-$O_2^{\bullet}$ strongly decrease. Through a Stern–Volmer treatment (eqn (3)) of the peroxyl lifetime *vs.*

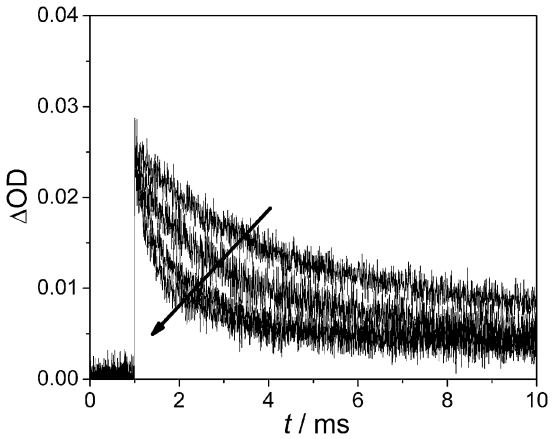

Fig. 11 Kinetic decays observed at 380 nm for TEA-$O_2^{\bullet}$ in a O_2 saturated solution of hexane–di-*tert* butyl peroxide (50 : 50 wt%) after the addition of, respectively 50, 350 and 950 μl of zirconium complex.

zirconium complex concentration, an "apparent" quenching rate constant of 1.6×10^3 $M^{-1}.s^{-1}$ can be obtained:

$$\frac{\tau_0}{\tau} = 1 + k_q \tau_0 [Q] \qquad (3)$$

where τ_0 is the lifetime (s) of the exited state in the absence of the quencher Q (zirconium complex) and k_q the quenching rate constant (M^{-1} s^{-1}).

This result is in agreement with the studies by Brindley *et al.*[51] on autoxidation of alkylzirconocenes of the type Cp_2ZrR_2 and $Cp_2Zr(R)X$ (Cp = π-cyclopentadienyl; R = methyl, benzyl or substituted benzyl; X = Cl or Br). It highlights that zirconium propoxide reacts with peroxyl radicals (resulting from the photoinitiator photolysis or growing chains) to give pentavalent alkoxides. These intermediate species lead, through molecular rearrangement, to the formation of $PrO^{\bullet}$, which are initiating species for the radical polymerisation. $PrO^{\bullet}$ can also abstract hydrogen atoms to create $R'^{\bullet}$ radicals that initiate a new chain reaction.

It should be mentioned that addition rate constants onto acrylate bonds are usually very low for peroxyl radicals and much higher for $RO^{\bullet}$. In light of these results, a general mechanistic approach between $Zr(OPr)_4$ and oxygen can be developed. This mechanism is described in Fig. 12.

In order to confirm this mechanism, molecular orbital calculations were carried out and simplified by replacing $Zr(OPr)_4$ by $Zr(OEt)_4$. When considering the geometry optimization of $ROO^{\bullet}Zr(OEt)_4$ through quantum mechanical calculations, the direct formation of the oxide ROO–$Zr(OEt)_3$ + $EtO^{\bullet}$ in Fig. 12 is observed. This shows that the cleavage process in this adduct radical is fast. Therefore, application of

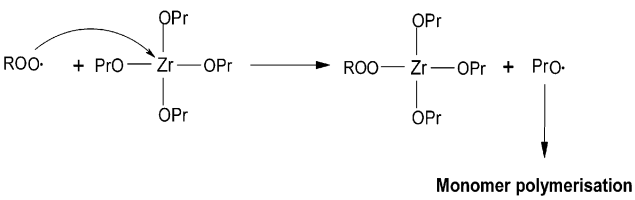

Fig. 12 Mechanistic approach between $RO_2^{\bullet}$ and zirconium propoxide; R is an organic group.

the mechanism from the model to the sol–gel system is possible. This model of reaction is one of the possible routes for the mechanistic reactions in sol–gel materials. However, other species (water, methanol,...) can affect the process and other radical reactions could be involved.

Conclusion

In this paper, atomic force microscopy in pulsed force mode coupled to real-time Fourier-transform infrared spectroscopy was successfully used to obtain information on surface chemical changes occurring during the free-radical photopolymerisation of hybrid sol–gel films containing metal alkoxides.

The pulsed force mode response was found to strongly depend on the $Zr(OPr)_4$/MAAH complex content: for the non-doped film, a signal corresponding to a very soft and sticky surface was reached. Addition of zirconium complex, even at low concentration, allows switching to a well-polymerised surface. It was demonstrated that the significantly different reactivity of the photopolymerisation to molecular oxygen, which is known to be a strong inhibitor, is linked to the presence of zirconium complex. One of the possible routes for the mechanistic reaction in sol–gel materials, under atmospheric conditions, has been proposed: radicals induced under UV irradiation react with O_2 to form peroxyl radicals, which add to Zr to form a $ROO^{\bullet}Zr(OR)_4$ complex. In a further step, $ROO^{\bullet}$ are converted into $RO^{\bullet}$ that acts as initiating species for free-radical induced photopolymerisation. This paper emphasizes a new method to reduce the detrimental effect of atmospheric oxygen in radical induced photopolymerisation. Since $Zr(OPr)_4$ acts on both the inorganic and the organic polymerisation, it is an attractive alternative compared to the conventional routes[52] involved to overcome O_2 inhibition and that usually consist of (a) adding a protective cover, (b) deactivating the irradiation setup with CO_2 or N_2, or (c) using specific oxygen scavengers such as amines or thiol compounds.

The approach developed in this paper can be assumed as general for radical induced polymerisation processes and will be developed in further studies.

References

1 G. Schottner, *Chem. Mater.*, 2001, **13**, 3422–3435.
2 J. Wen and G. L. Wilkes, *Chem. Mater.*, 1996, **8**, 1667–1681.
3 P. F. Simon, R. Ulrich, H. W. Spiess and U. Wiesner, *Chem. Mater.*, 2001, **13**, 3464–3486.
4 C. Sanchez, B. Lebeau, F. Ribot and M. In, *J. Sol–Gel Sci. Technol.*, 2000, **19**, 31–38.
5 C. Sanchez, B. Julian, P. Belleville and M. Popall, *J. Mater. Chem.*, 2005, **15**, 3559–3592.
6 J. D. Mackenzie and E. Bescher, *J. Sol–Gel Sci. Technol.*, 2002, **27**, 7–14.
7 M. Toselli, M. Marini, P. Fabbri, M. Messori and F. Pilati, *J. Sol–Gel Sci. Technol.*, 2007, **43**, 73–83.
8 M. E. L. Wouters, D. P. Wolfs, M. C. Van der Linde, J. H. P. Hovens and A. H. A. Tinnemans, *Prog. Org. Coat.*, 2004, **51**, 312–320.
9 S. Hofacker, M. Mechtel, M. Mager and H. Kraus, *Prog. Org. Coat.*, 2002, **45**, 159–164.
10 M. Messori, M. Toselli, F. Pilati, P. Fabbri, L. Pasquali and S. Nannarone, *Polymer*, 2004, **45**, 805–813.
11 M. Quinet, B. Neveu, V. Moutarlier, P. Audebert and L. Ricq, *Prog. Org. Coat.*, 2007, **58**, 46–53.
12 M. L. Zheludkevich, R. Serra, M. F. Montemor, I. M. Miranda Salvado and M. G. S. Ferreira, *Surf. Coat. Technol.*, 2006, **200**, 3084–3094.
13 X. F. Yang, D. E. Tallman, V. J. Gelling, G. P. Bierwagen, L. S. Kasten and J. Berg, *Surf. Coat. Technol.*, 2001, **140**, 44–50.
14 S. Amberg-Schwab, H. Katschorek, U. Weber, A. Burger, R. Hansel, B. Steinbrecher and D. Harzer, *J. Sol–Gel Sci. Technol.*, 2003, **26**, 699–703.
15 S. Amberg-Schwab, H. Katschorek, U. Weber, M. Hoffmann and A. Burger, *J. Sol–Gel Sci. Technol.*, 2000, **19**, 125–129.
16 S. Amberg-Schwab, M. Hoffmann, H. Bader and M. Gessler, *J. Sol–Gel Sci. Technol.*, 1998, **1/2**, 141–146.
17 P. Etienne, P. Coudray, Y. Moreau and J. Porque, *J. Sol–Gel Sci. Technol.*, 1998, **13**, 523–527.
18 M. Oubaha, P. Etienne, S. Calas, P. Coudray, J. M. Nedelec and Y. Moreau, *J. Sol–Gel Sci. Technol.*, 2005, **33**, 241–248.
19 C. Molina, P. J. Moreira, R. R. Gonçalves, R. A. S. Ferreira, Y. Messaddeq, S. J. L. Ribeiro, O. Soppera, A. P. Leite, P. V. S. Marques, V. de Zea Bermudez and L. D. Carlos, *J. Mater. Chem.*, 2005, **15**, 3937–3945.
20 M. Marini, S. De Niederhausern, R. Iseppi, M. Bondi, C. Sabia, M. Toselli and F. Pilati, *Biomacromolecules*, 2007, **8**, 1246–1254.
21 C. Sanchez and F. Ribot, *New J. Chem.*, 1994, **18**, 1007–1047.
22 O. Soppera, C. Croutxé-Barghorn and D. J. Lougnot, *New J. Chem.*, 2001, **25**, 1006–1014.
23 O. Soppera and C. Croutxé-Barghorn, *J. Polym. Sci., Part A: Polym. Chem.*, 2003, **41**, 716–724.
24 O. Soppera and C. Croutxé-Barghorn, *J. Polym. Sci., Part A: Polym. Chem.*, 2003, **41**, 831–840.
25 C. Coutxé-Barghorn and O. Soppera, *J. Sol–Gel Sci. Technol.*, 2007, **41**, 93–97.
26 W. S. Kim, R. Houbertz, T. H. Lee and B. S. Bae, *J. Polym. Sci., Part A: Polym. Chem.*, 2004, **42**, 1979–1986.
27 R. Houbertz, G. Domann, J. Schulz, B. Olsowski, L. Frohlich and W. S. Kim, *Appl. Phys. Lett.*, 2004, **84**, 1105–1107.
28 J. Urreaga, M. Matias, V. Lorenzo and M. U. d. l. Orden, *Mater. Lett.*, 2000, **45**, 293–297.
29 D. Blanc, A. Last, J. Franc, S. Pavan and J. L. Loubet, *Thin Solid Films*, 2006, **515**, 942–946.
30 O. Soppera, M. Feuillade, C. Croutxé-Barghorn and C. Carré, *Prog. Solid State Chem.*, 2005, **33**, 233–242.
31 S. Jradi, O. Soppera and D. J. Lougnot, *J. Microsc.*, 2008, **229**, 151–161.
32 R. D. Maggio, L. Fambri, M. Cesconi and W. Vaona, *Macromolecules*, 2002, **35**, 5342–5344.
33 P. Dobrzynski, *J. Polym. Sci., Part A: Polym. Chem.*, 2003, **42**, 1886–1900.
34 A. Rosa-Zeiser, E. Weilandt, S. Hild and O. Marti, *Meas. Sci. Technol.*, 1997, **8**, 1333–1338.
35 J. Lalevée, X. Allonas and J. P. Fouassier, *J. Am. Chem. Soc.*, 2002, **124**, 9613–9621.
36 T. Scherzer and U. Decker, *Vib. Spectrosc.*, 1999, **19**, 385–398.
37 C. Decker and K. Moussa, *Polym. Mater. Sci. Eng.*, 1986, **55**, 552–556.
38 C. Decker and K. Moussa, *J. Eur. Polym.*, 1990, **26**, 393–401.
39 D. Massiot, F. Fayon, M. Capron, I. King, S. L. Calvé, B. Alonso, J. O. Durand, B. Bujoli, Z. Gan and G. Hoatson, *Magn. Reson. Chem.*, 2002, **40**, 70–76.
40 J. Lalevée, X. Allonas and J. P. Fouassier, *Chem. Phys. Lett.*, 2007, **445**, 62–67.
41 M. J. Frisch, G. W. Trucks, H. B. Schlegel, G. E. Scuseria, M. A. Robb, J. R. Cheeseman, V. G. Zakrzewski, J. A. Montgomery, Jr., R. E. Stratmann, J. C. Burant, S. Dapprich, J. M. Millam, A. D. Daniels, K. N. Kudin, M. C. Strain, O. Farkas, J. Tomasi, V. Barone, M. Cossi, R. Cammi, B. Mennucci, C. Pomelli, C. Adamo, S. Clifford, J. Ochterski, G. A. Petersson, P. Y. Ayala, Q. Cui, K. Morokuma, P. Salvador, J. J. Dannenberg, D. K. Malick, A. D. Rabuck, K. Raghavachari, J. B. Foresman, J. Cioslowski, J. V. Ortiz, A. G. Baboul, B. B. Stefanov, G. Liu, A. Liashenko, P. Piskorz, I. Komaromi, R. Gomperts, R. L. Martin, D. J. Fox, T. Keith, M. A. Al-Laham, C. Y. Peng, A. Nanayakkara, M. Challacombe, P. M. W. Gill, B. G. Johnson, W. Chen,

M. W. Wong, J. L. Andres, C. Gonzalez, M. Head-Gordon, E. S. Replogle and J. A. Pople, *GAUSSIAN 98 (Revision A.11)*, Gaussian, Inc., Pittsburgh, PA, 2001.
42 M. Oubaha, P. Etienne, S. Calas, R. Sempere, J. M. Nedelec and Y. Moreau, *J. Non-Cryst. Solids*, 2005, **351**, 2122–2128.
43 K. Saravanamuttu, X. M. Du, S. I. Najafi and M. P. Andrews, *Can. J. Chem.*, 1998, **76**, 1717–1729.
44 M. Feuillade, in Département de Photochimie Générale, Université de Mulhouse, 2005, p. 270.
45 H. Hayashi, H. Suzuki and S. Kaneko, *J. Sol–Gel Sci. Technol.*, 1998, **12**, 87–94.
46 H. Sayilkan, S. Sener, E. Sener and E. Arparc, *J. Mater. Sci.*, 1999, **34**, 5325–5330.
47 U. Schubert, E. Arpac, W. Glaubitt, A. Helmerich and C. Chau, *Chem. Mater.*, 1992, **4**, 291–295.
48 L. Delattre, M. Roy and F. Babonneau, *J. Sol–Gel Sci. Technol.*, 1997, **8**, 567–570.
49 L. Delattre and F. Babonneau, *Chem. Mater.*, 1997, **9**, 2385–2394.
50 H. Fischer, in *Radical Reaction Rates in Liquid Peroxyl and Related Radicals*, Springer Verlag, Berlin, 1997Subvol. 2.
51 P. B. Brindley and M. J. Scotton, *J. Chem. Soc., Perkin Trans. 2*, 1981, 419–423.
52 R. S. Davidson, in *Radiation Curing in Polymer Science and Technology-Volume III Polymerization Mechanism*, ed. J. P. Fouassier and J. F. Rabek, Elsevier Applied Science, London, 1993.

